The Astrophysical Journal Letters, 892:L8 (5pp), 2020 March 20 https://doi.org/10.3847/2041-8213/ab7cdc


# The Branching Ratio of LIGO Binary Black Holes

Mohammadtaher Safarzadeh[1,2]
[1] Center for Astrophysics|Harvard & Smithsonian, 60 Garden Street, Cambridge, MA, USA; msafarzadeh@cfa.harvard.edu
[2] Department of Astronomy and Astrophysics, University of California, Santa Cruz, CA 95064, USA
*Received 2020 February 11; revised 2020 March 3; accepted 2020 March 4; published 2020 March 20*

## Abstract

Formation of binary black holes (BBHs) detected by gravitational-wave observations could be broadly divided into two categories: those formed through field binary evolution and those assembled dynamically in dense stellar systems. The branching ratio of the BBHs refers to the contribution of each channel. The dynamical assembly channel would predict a symmetric distribution in the effective spins of the BBHs while field formation predicts BBHs to have positive effective spins. By modeling these two populations based on their effective spin distribution we show that in the 10 BBHs detected by LIGO/Virgo the contribution of the dynamically assembled BBHs is more than about 50% with 90% confidence. This result is based on the assumption that the field binaries are born with positive effective spins not restricted to have small values.

*Unified Astronomy Thesaurus concepts:* LIGO (920); Black hole physics (159); High energy astrophysics (739)

## 1. Introduction

The effective spin of a binary black hole (BBH) system is defined as

$$\chi_{\rm eff} \equiv \frac{m_1 a_1 \cos(\theta_1) + m_2 a_2 \cos(\theta_2)}{m_1 + m_2}, \quad (1)$$

where $m_1$ and $m_2$ are the masses of the primary and secondary black hole, and $a_1$ and $a_2$ their associated dimensionless spin magnitude defined as

$$a = \frac{cJ_{\rm BH}}{GM^2{}_{\rm BH}}. \quad (2)$$

Here $c$ is the speed of light, $G$ is the gravitational constant, and $M_{\rm BH}$ and $J_{\rm BH}$ are the mass and angular momentum (AM) of the BH. $\theta$ is the angle between the direction of each BH's spin and the orbital AM of the BBH. The effective spin parameter is the best-measured spin-related parameter from gravitational-wave observations (Farr et al. 2017 and references therein).

The expected spin of a newly born BH depends on the efficiency of AM transfer from the core of its progenitor star's core to outer shell layers through magnetic fields. Models assuming moderate efficiency of AM transport through meridional currents predict the formation of BHs with high spins (Eggenberger et al. 2007; Ekström et al. 2011), while efficient transport by the Tayler–Spruit magnetic dynamo (Spruit 1999, 2001), as implemented in stellar evolution calculations (Fuller et al. 2019; Fuller & Ma 2019), predicts all BHs to be born very slowly rotating.

Therefore, the effective spin distribution of the BBHs observed with LIGO/Virgo (hereafter LIGO BBHs) illuminates their formation process (Farr et al. 2017; Stevenson et al. 2017; Vitale et al. 2017). Broadly, LIGO BBHs may be divided into two categories: (i) assembled in the field through stellar evolution and a potential common-envelope phase. Such binaries are expected to have their BH spins preferentially aligned with the orbital AM of the binary (Belczynski et al. 2002; Dominik et al. 2012; Zaldarriaga et al. 2017; Hotokezaka & Piran 2017; Gerosa et al. 2018; Qin et al. 2018; Schrøder et al. 2018; Bavera et al. 2019); (ii) assembled dynamically, either in globular or nuclear star clusters or hierarchical triple or higher-order stellar systems (Zwart et al. 2004; Samsing et al. 2014, 2018; Chatterjee et al. 2016; Rodriguez et al. 2016, 2018; Antonini et al. 2017). Such binaries are expected to have their spin isotropically distributed with respect to the AM of the binary and therefore result in the symmetric distribution in $\chi_{\rm eff}$.

While the effective spin parameter for the 10 LIGO/Virgo GWTC-1 BBHs is consistent with being clustered around zero (Belczynski et al. 2017; Abbott et al. 2019b; Roulet & Zaldarriaga 2019) recent work by Safarzadeh et al. (2020a) indicates a trend in the distribution suggestive of a nonnegligible contribution from dynamically assembled binaries. In this Letter we analyze the same set of BBHs searching for the contribution of field binaries.

## 2. Method

The method is based on the assumption that dynamically assembled binaries will have symmetric distribution in $\chi_{\rm eff}$ while field binaries will prefer to have a predominantly positive $\chi_{\rm eff}$ distribution. Although this assumption is broadly expected to be the case, there are mechanisms in the field formation scenario that can result in a negative effective spin (Gerosa et al. 2018) that we do not consider in the present work. If we denote the number of BBHs with positive (negative) $\chi_{\rm eff}$ with $N_p$ ($N_n$), the fraction of BBHs coming from field population could be defined as

$$Q = \frac{N_p - N_n}{N_p + N_n}. \quad (3)$$

Although dynamical assembly of the BBHs would predict symmetric distribution in $\chi_{\rm eff}$, LIGO's sensitivity for the detection of a BBH is not insensitive to their $\chi_{\rm eff}$. Figure 1 shows the detection probability of a population of BBHs with $P(m_1) \propto m_1^{-1}$ and $p(m_2|m_1) \propto$ const and each component mass range between 5 and 50 $M_\odot$. For LIGO it is easier to detect BBHs with positive $\chi_{\rm eff}$ than their negative counterparts (Ng et al. 2018), and therefore even if all the BBHs are assembled dynamically, LIGO would be biased toward those with positive $\chi_{\rm eff}$ making the final distribution in mass–$\chi_{\rm eff}$ plane asymmetric.

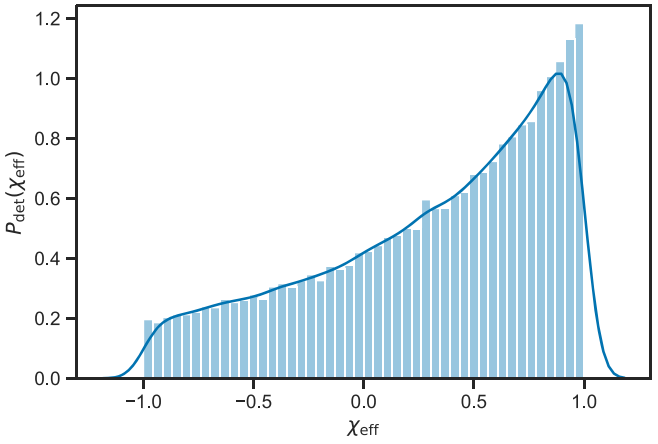


**Figure 1.** Detection probability for $\chi_{\rm eff}$ for a population of BBHs with $P(m_1) \propto m_1^{-1}$ and $p(m_2|m_1) \propto$ const between 5 and 50 solar mass. See Safarzadeh et al. (2020a) for details.

Therefore, the formula above would need to be corrected for the selection bias of LIGO. When analyzing LIGO BBHs we instead use the effective $N_p$ and $N_n$ defined as

$$\langle N_p \rangle = \sum_{i=0}^{i=N_{\rm BBH}} P_{\rm det}^{-1}(\chi_{\rm eff}^i)\mathcal{H}(\chi_{\rm eff}^i) \quad (4)$$

and

$$\langle N_n \rangle = \sum_{i=0}^{i=N_{\rm BBH}} P_{\rm det}^{-1}(\chi_{\rm eff}^i)\mathcal{H}(-\chi_{\rm eff}^i), \quad (5)$$

where $\mathcal{H}(x)$ is Heaviside step function returning one if the argument is positive and zero otherwise.

If we have a set of $N$ BBHs, by sampling $N_s$ times from their posterior distribution in mass and $\chi_{\rm eff}$, we can have $N_s$ times measurement of the parameter $Q$ and construct a probability distribution for $Q$. We adopt $N_s = 100$ for testing purposes and $N_s = 1000$ for analyzing LIGO data. We do this by sampling with replacement to remove potential bias from individual BBHs in the sample, specifically important when the sample size is small.

To test the method, we first construct a set of mock distribution of BBHs in the $\chi_{\rm eff}$–mass plane. After defining the total number of the BBHs and $Q$, the total number of the field BBHs is set through a binomial distribution $N_f = \binom{N_{\rm BBH}}{Q}$, and the total number of dynamically assembled binaries is $N_d = N_{\rm BBH} - N_f$. For all binaries we assume a uniform distribution in chirp mass between 10 and 50 $M_\odot$. For field binaries we assume a uniform distribution in $\chi_{\rm eff} \in [0, 1]$. For the dynamically assembled binaries we consider a normal distribution $\mathcal{N}(0, \sigma)$ with $\sigma = \alpha(M_c/5)$, where $M_c$ is the chirp mass of the binary in solar units. Such a distribution would populate dynamically assembled binaries symmetrically in $\chi_{\rm eff}$ around zero with its dispersion increasing with mass. We set a fiducial value of $\alpha = 0.1$; however, our result is not sensitive to the exact choice of this parameter. The increase of dispersion is due to a random walk in $\chi_{\rm eff}$–mass that higher-generation BHs follow. After populating the BBHs in the mass–$\chi_{\rm eff}$ plane, we assume their posterior probability distribution function (PDF) in mass and $\chi_{\rm eff}$ follows a normal distribution with $\sigma_{\chi_{\rm eff}} = 0.1$, and $\sigma_M = 1M_\odot$, which is similar to the dispersion in the posterior distribution on mass and $\chi_{\rm eff}$ of the first 10 LIGO BBHs (Abbott et al. 2019a). When sampling from the $\chi_{\rm eff}$ PDF of the BBHs, we impose a minimum and maximum of −1 and 1 for the $\chi_{\rm eff}$.

Figure 2 shows three different mock distribution where their true $Q$ is shown with a dashed black line. In each panel, we simulate $N_{\rm BBH}$ mock BBH observations, and determine the recovered $Q$ parameter. In the top (bottom) row we set $N_{\rm BBH} = 10$ (30). We repeat this process 100 times, and show each realization with a different color in Figure 2. The black solid line shows the stack of all the colored lines, indicating the overall power of recovering the true $Q$ when the number of the BBHs is considered to be 10. We note that in this computation the selection bias of LIGO in detecting BBHs with different $\chi_{\rm eff}$ is not modeled.

The summary of our results is presented in the probability–probability plot ($p$–$p$ plot) shown in Figure 3. This plot shows the fraction of simulated BBH distributions with $Q$ values within a credible interval as a function of credible interval. If our parameter estimation method is unbiased, one expects to recover the black solid diagonal line that indicates the ideal 1-to-1 relation. The blue curve shows our results. We have done the following steps: (i) Draw $N_{\rm inj} = 1000$ $Q$ values from a uniform prior between 0 and 1. (ii) Generate mock data set: draw $N_{\rm BBH}$ BBHs from the mixture model described in Section 2 with a true value of $Q$. (iii) Produce posterior on $Q$ for each of the $N_{\rm inj}$. (iv) Determine at which credible interval the true injected value of $Q$ falls within each mock posterior. (v) For each credible interval between 0 and 1, compute the fraction of events that contain the true value within that credible interval. The blue (orange) line in Figure 3 indicates the result when $N_{\rm BBH} = 10$ (30). As can be seen the relationship we get for $N_{\rm BBH} = 10$ is close to a 1-to-1 relation but the result for $N_{\rm BBH} = 30$ deviates from it, and therefore our parameter estimation is biased in the sense that we tend to *underestimate* $Q$.

The source of the bias lies in the magnitude of the error we consider for $\chi_{\rm eff}$. Throughout this Letter we have assumed $\sigma_{\chi_{\rm eff}} = 0.1$ based on the LIGO GWTC-1 catalog. When sampling from the posterior distribution of a BBH's $\chi_{\rm eff}$, the sampled realization can have a negative $\chi_{\rm eff}$ value depending on the magnitude of the BBH's mean $\chi_{\rm eff}$. Since in this formalism any BBH with negative $\chi_{\rm eff}$ is considered to be coming from a dynamical channel, we will be biased to underestimate the contribution of the field binaries. For example, if we adopt a $\sigma_{\chi_{\rm eff}} = 0.01$ for the BBHs, we would not see a bias in the results. The impact of this bias is more pronounced when the sample size is increased. Moreover, if we assume that field binaries are all born with small positive effective spins (e.g., $\chi_{\rm eff} < 0.1$), results from our method would be greatly biased in favor of dynamically assembled binaries because of the current effective spin error magnitude considered in this work (i.e., $\sigma_{\chi_{\rm eff}} = 0.1$).

In order to quantify the level of bias in our method, we perform the following test: (i) Draw $N_{\rm inj} = 1000$ $Q$ values from a uniform prior between 0 and 1. (ii) Produce posterior on $Q$ for each of the $N_{\rm inj}$. The posterior on $Q$, however, is assumed to be a normal distribution centered on $Q$ with a standard deviation of $\sigma_t = 0.5$. (iii) We reassign the true value of $Q$ by drawing from the posterior we made in the previous step. (iv) In order to make the result biased, we shift the true $Q$ value from the previous step by $\delta Q$. (v) Determine at which credible interval the true injected value of $Q$ falls within each mock posterior and plot the $p$–$p$ plot. We assume $\delta Q$ to be 0.05 (0.1) and the result is shown with a dashed green (dotted red) line in Figure 3. As can be seen the orange line in Figure 3 lies

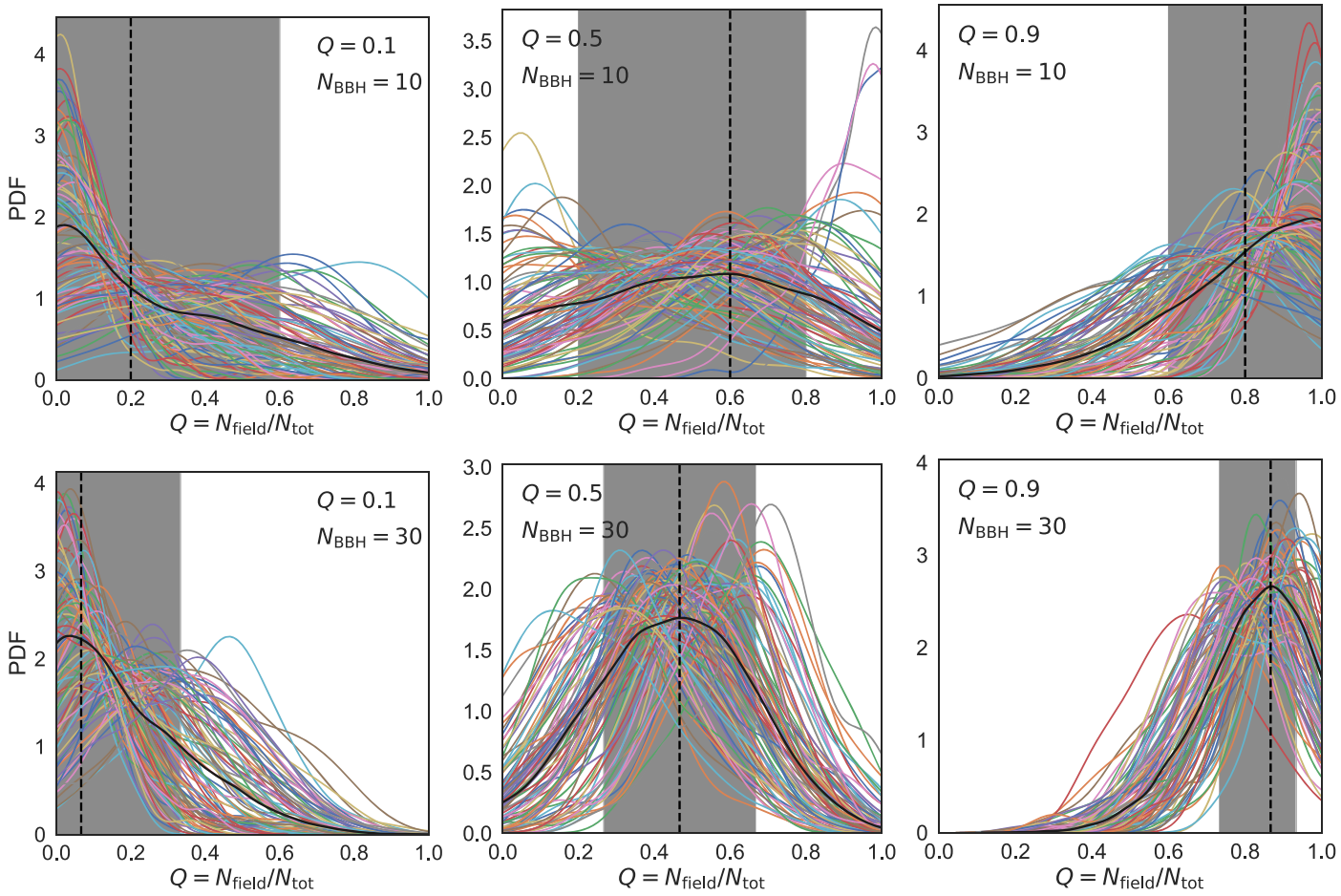


**Figure 2.** Top row: posterior distribution on the parameter $Q$, which indicates the contribution fraction of field binaries to the overall mock BBH distributions. Each colored line shows the posterior of $Q$ for a given random distribution of $N_{\rm BBH} = 10$ BBHs in the mass–$\chi_{\rm eff}$ plane. The black solid lines show the stack of the colored lines. The shaded region shows the 16th and 84th percentiles, and the black dashed line shows the median value of the black PDF. Note that the dashed vertical black line does *not* indicate the true $Q$ value.The true $Q$ is mentioned in each panel. We note that in this computation the selection bias of LIGO in detecting BBHs with different $\chi_{\rm eff}$ is not modeled. Bottom row: same as the top row, but when the $N_{\rm BBH} = 30$.

between the results where we impose 5% and 10% bias in underestimating the truth. We note that in the above test, we are not sensitive to the exact choice of $\sigma_t$. For example, adopting $\sigma_t = 0.1$ (meaning a narrow PDF for the posterior on $Q$) would make our result consistent with a bias of less than 5%, while a larger value of $\sigma_t$ would not increase the bias above 10%.

## 3. GWTC-1 Result

In this section, we present our result on the catalog of the first 10 BBHs observed by the LIGO Scientific Collaboration (LSC;[3] Abbott et al. 2019a). Figure 4 shows the posterior distribution for $Q$. In the solid black line we show the result of taking into account the detection probability function of LIGO as a function of $\chi_{\rm eff}$ and analyzing all 10 LIGO BBHs. Our results indicate that the contribution from the dynamical channel is more than ≈55% with 90% confidence. In the dashed black line we show the same result when excluding GW170729 from the analysis since this BBH merger event has the highest false-alarm rate among all. We see that our result is not driven by GW170729, although excluding this event slightly increases the contribution of the dynamical channel to the overall statistics.

[3] See https://dcc.ligo.org/LIGO-P1800370/public.

We note that if the field binaries are all born with very small positive effective spin, the likelihood of considering them as dynamically assembled increases given the current level of uncertainty on effective spin $\sigma_{\chi_{\rm eff}} \approx 0.1$. In this case our method would be biased in favor of dynamically assembled binaries unless the posterior that LIGO provides for such sources are smaller than their mean effective spin magnitude.

## 4. Summary and Conclusion

BBHs observed by LIGO/Virgo are expected to populate different areas in the $\chi_{\rm eff}$–mass plane depending on their formation channel Field binaries tend to predict a largely positive $\chi_{\rm eff}$ distribution while dynamical assembly of BBHs in dense stellar clusters leads to a symmetric distribution of BBHs in $\chi_{\rm eff}$ at all masses with larger dispersion at higher masses. The increase of dispersion is due to a random walk in $\chi_{\rm eff}$–mass that higher-generation BHs follow.

In Safarzadeh et al. (2020a) we found a tentative negative correlation between $\chi_{\rm eff}$ and chirp mass for the 10 LIGO/Virgo BBHs with ∼75% confidence. Moreover, we found that the dispersion in $\chi_{\rm eff}$ grows with mass with 80% confidence. These trends are consistent with a combined channel of dynamically assembled BBHs that provide the positive trend of dispersion

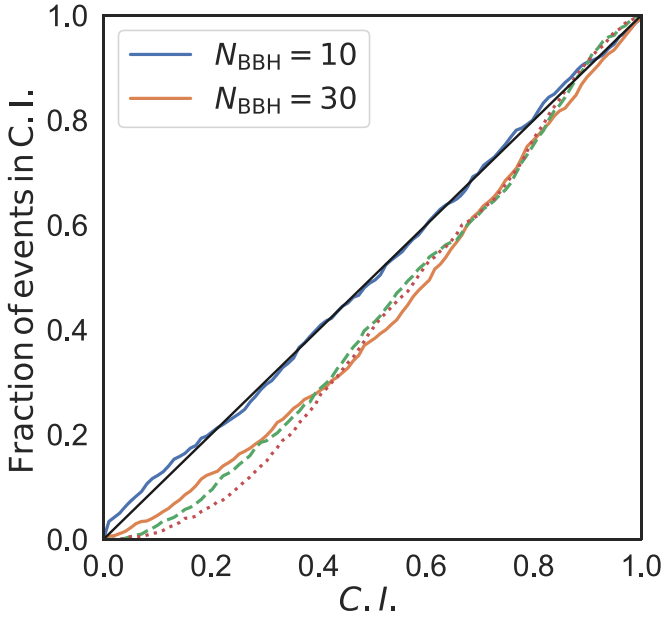


**Figure 3.** Faction of simulated BBH distributions with $Q$ values within a credible interval as a function of credible interval. If our parameter estimation method is unbiased, one expects to recover the black solid diagonal line that indicates the ideal 1-to-1 relation. The blue line shows our results from 1000 simulation of a set of 10 BBHs with random underlying $Q$ values. This result indicates that on average we underestimate the true input $Q$. The dashed green (dotted red) line shows the test result when we impose a bias of 5% (10%), respectively. This shows that the bias in our method lies between 5%–10%.

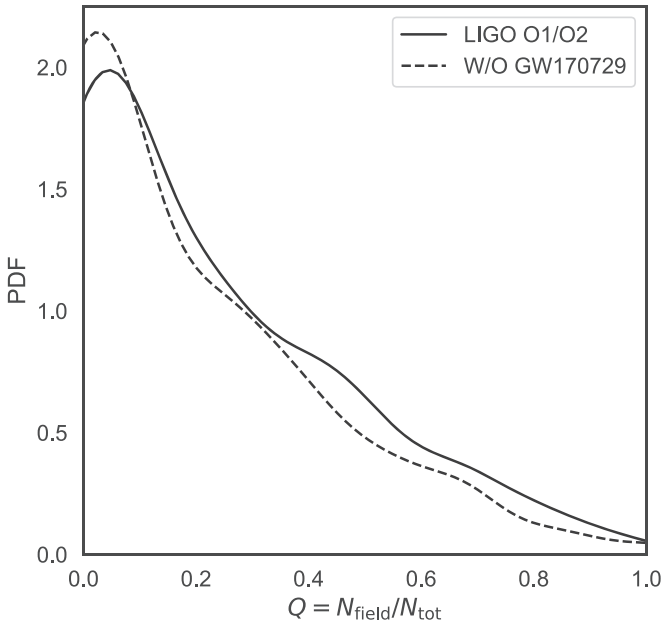


**Figure 4.** Posterior distribution on the parameter $Q$, which indicates the contribution fraction of field binaries to the overall BBH observed with LSC. In the solid black line we show the result for all the 10 BBHs, and in the dashed black line we have excluded GW170729 from the analysis given this BBH has the highest false-alarm rate. Both lines are smoothed KDE representation of the results. Our results indicate that the contribution from the dynamical channel is more than ≈55% with 90% confidence, and excluding GW170729 does not have a significant impact on the overall statistics.

with mass, and a field formation channel that provides the negative mean trend with mass could explain our findings.

In this Letter we took a different approach to characterize the branching ratio of the LIGO BBHs. The fundamental assumption in this work is that dynamically assembled BBHs will be distributed symmetrically in $\chi_{\rm eff}$ (prior to correcting for the LIGO detection bias of the BBHs as a function of their $\chi_{\rm eff}$), while BBHs formed through field binary evolution will end up as having a positive $\chi_{\rm eff}$ although each subchannel will populate a distinct region in $\chi_{\rm eff}$–mass plane. We note that the analysis itself is only carried out in effective spin dimension and not in the $\chi_{\rm eff}$–mass plane.

We show that there is a support for the symmetric distribution in $\chi_{\rm eff}$ (which is the tracer of the dynamical formation channel) to be more than 55% with 90% confidence. This result is not sensitive to the presence of GW170729, which is a particular high-spin event in the catalog and is in line with the findings in Safarzadeh et al. (2020a). By taking a rather different approach, while having the same goal as the work presented here, Farr et al. (2018) analyzed the first four LIGO BBHs and concluded that the odds of them being formed from field distribution over dynamically assembled origin is 1.1. Implementing a hierarchical Bayesian approach (Abbott et al. 2019) show that the data prefer a dynamical assembly origin for the LIGO BBHs; however, assuming the intrinsic effective spins are clustered around zero would significantly reduce our ability to distinguish between the two formation channels. Explaining the LIGO BBHs with the latest catalogs of population synthesis models and $N$-body codes, Bouffanais et al. (2019) conclude that the data are barely consistent (still consistent) with a model in which all the BBHs are born in the field (clusters), a result that would depend on the metallicity distribution of the BBH progenitors (Safarzadeh & Farr 2019).

Our approach in this work is simple with basic assumptions about effective spin distribution of the BBHs. We show that such simple assumptions lead to conclusions that are consistent with previous Bayesian modeling of the 10 LIGO BBHs. Other considerations can in principle be incorporated in such analysis: for example if the LSC detects a BBH with mass above the pair-instability mass gap (Woosley 2017), the likelihood of such BBH to belong to the dynamical formation channel would be increased. Likewise, high mass ratio systems are likely formed in the field since such systems cannot be effectively assembled in clusters due to mass segregation (see Safarzadeh et al. 2020b and references therein). Future O3 data releases will confirm this finding as the number of events is expected to be around 30, which increases the overall sensitivity by about a factor of 2.

M.T.S. is thankful to the referee for constructive comments. M.T.S. is thankful to Avi Loeb for asking about the branching ratio of the LIGO BBHs, which inspired this work. M.T.S. is also thankful to Will M. Farr, Enrico Ramirez-Ruiz, and Ryan Foley for insightful discussions. M.T.S. thanks the Heising-Simons Foundation, the Danish National Research Foundation (DNRF132), and NSF (AST-1911206 and AST-1852393) for support. This material is based upon work supported by the National Science Foundation under grant No. AST-1440254.

*Software:* Numpy (Walt et al. 2011), Scipy (Virtanen et al. 2020), IPython (Pérez & Granger 2007), Matplotlib (Hunter 2007).

## References

Abbott, B., Abbott, R., Abbott, T., et al. 2019a, PhRvX, 9, 031040
Abbott, B. P., Abbott, R., Abbott, T. D., et al. 2019b, ApJL, 882, L24
Antonini, F., Rodriguez, C. L., Petrovich, C., & Fischer, C. L. 2017, MNRAS Letters, 480, L58
Bavera, S. S., Fragos, T., Qin, Y., et al. 2019, arXiv:1906.12257

Belczynski, K., Kalogera, V., & Bulik, T. 2002, ApJ, 572, 407
Belczynski, K., Klencki, J., Fields, C. E., et al. 2017, arXiv:1706.07053
Bouffanais, Y., Mapelli, M., Gerosa, D., et al. 2019, ApJ, 886, 25
Chatterjee, S., Rodriguez, C. L., Kalogera, V., & Rasio, F. A. 2016, ApJL, 836, L26
Dominik, M., Belczynski, K., Fryer, C., et al. 2012, ApJ, 759, 52
Eggenberger, P., Meynet, G., Maeder, A., et al. 2007, Ap&SS, 316, 43
Ekström, S., Georgy, C., Eggenberger, P., et al. 2011, A&A, 537, A146
Farr, B., Holz, D. E., & Farr, W. M. 2018, ApJL, 854, L9
Farr, W. M., Stevenson, S., Miller, M. C., et al. 2017, Natur, 548, 426
Fuller, J., & Ma, L. 2019, ApJL, 881, L1
Fuller, J., Piro, A. L., & Jermyn, A. S. 2019, MNRAS, 485, 3661
Gerosa, D., Berti, E., O'Shaughnessy, R., et al. 2018, PhRvD, 98, 084036
Hotokezaka, K., & Piran, T. 2017, ApJ, 842, 111
Hunter, J. D. 2007, CSE, 9, 90
Ng, K. K. Y., Vitale, S., Zimmerman, A., et al. 2018, PhRvD, 98, 083007
Pérez, F., & Granger, B. E. 2007, CSE, 9, 21
Qin, Y., Marchant, P., Fragos, T., Meynet, G., & Kalogera, V. 2018, ApJL, 870, L18
Rodriguez, C. L., Amaro-Seoane, P., Chatterjee, S., et al. 2018, PhRvD, 98, 123005
Rodriguez, C. L., Zevin, M., Pankow, C., Kalogera, V., & Rasio, F. A. 2016, ApJL, 832, L2
Roulet, J., & Zaldarriaga, M. 2019, MNRAS, 484, 4216
Safarzadeh, M., & Farr, W. M. 2019, ApJL, 883, L24
Safarzadeh, M., Farr, W. M., & Ramirez-Ruiz, E. 2020a, arXiv:2001.06490
Safarzadeh, M., Hamers, A. S., Loeb, A., & Berger, E. 2020b, ApJL, 888, L3
Samsing, J., MacLeod, M., & Ramirez-Ruiz, E. 2014, ApJ, 784, 71
Samsing, J., MacLeod, M., & Ramirez-Ruiz, E. 2018, ApJ, 853, 140
Schrøder, S. L., Batta, A., & Ramirez-Ruiz, E. 2018, ApJL, 862, L3
Spruit, H. C. 1999, A&A, 349, 189
Spruit, H. C. 2001, A&A, 381, 923
Stevenson, S., Berry, C. P. L., & Mandel, I. 2017, MNRAS, 471, 2801
Virtanen, P., Gommers, R., Oliphant, T. E., et al. 2020, Nature Methods, 17, 261
Vitale, S., Lynch, R., Sturani, R., & Graff, P. 2017, CQGra, 34, 03LT01
Walt, S. V. d., Colbert, S. C., & Varoquaux, G. 2011, CSE, 13, 22
Woosley, S. E. 2017, ApJ, 836, 244
Zaldarriaga, M., Kushnir, D., & Kollmeier, J. A. 2017, MNRAS, 473, 4174
Zwart, S. P., Baumgardt, H., Hut, P., Makino, J., & McMillan, S. 2004, Natur, 428, 724